LETTER

Dielectric meta-walls for surface plasmon focusing and Bessel beam generation

To cite this article: Shaohua Dong *et al* 2018 *EPL* **122** 67002

A Letters Journal Exploring the Frontiers of Physics

June 2018

EPL, **122** (2018) 67002
doi: 10.1209/0295-5075/122/67002

www.epljournal.org

Dielectric meta-walls for surface plasmon focusing and Bessel beam generation

Shaohua Dong[1(a)], Zhuo Wang[2(a)], Huijie Guo[2], Fuxin Guan[2], Xiaoer Li[1], Qiong He[2,3], Haibin Zhao[1], Lei Zhou[2,3] and Shulin Sun[1,4(b)]

[1] *Shanghai Engineering Research Center of Ultra-Precision Optical Manufacturing, Green Photonics and Department of Optical Science and Engineering, Fudan University - Shanghai 200433, China*
[2] *State Key Laboratory of Surface Physics and Key Laboratory of Micro and Nano Photonic Structures (Ministry of Education), Fudan University - Shanghai 200433, China*
[3] *Collaborative Innovation Center of Advanced Microstructures - Nanjing 210093, China*
[4] *State Key Laboratory of Applied Optics, Changchun Institute of Optics, Fine Mechanics and Physics, Chinese Academy of Sciences - Changchun 130033, China*

received 4 June 2018; accepted in final form 3 July 2018
published online 25 July 2018

PACS 78.67.Pt – Multilayers; superlattices; photonic structures; metamaterials
PACS 42.79.-e – Optical elements, devices, and systems
PACS 73.20.Mf – Collective excitations (including excitons, polarons, plasmons and other charge-density excitations)

Abstract – Freely tailoring the wavefronts of surface plasmon polaritons (SPPs) is a central goal in plasmonics, but the conventional approaches exhibit low efficiencies and/or require bulky devices. Here, we propose to utilize ultrathin dielectric meta-walls placed vertically on a plasmonic metal to efficiently reshape the wavefront of a launched SPP beam. Based on such a strategy, we experimentally demonstrate two effects in the microwave regime, namely focusing and Bessel beam generations of spoof SPPs. Near-field scanning measurements are in excellent agreement with full wave simulations. This work can stimulate research in many applications related to SPP manipulations, such as enhanced nonlinear effect, nano-particle trapping, and so on.

Surface plasmon polaritons (SPPs), electromagnetic (EM) eigenmodes bounded on dielectric/metal interfaces coupled with the free-electron oscillations inside metals, play vital roles in photonic research. The two important characteristics of SPP modes, *i.e.*, their subwavelength resolution and local field enhancement, grant them potential for numerous applications, including the super-resolution imaging [1], enhanced nonlinear effect [2,3], lasing spaser [4], on-chip photonic circuits [5], etc. A fundamental scientific issue in these applications is how to control the wavefronts of SPPs freely and efficiently. To achieve this goal, people have employed dielectric disks [6,7] and plasmonic photonic crystals [8,9] to realize SPP focusing and reflection (see figs. 1(a), (b)), based on similar mechanisms for controlling space waves. Moreover, periodic or non-periodic nanostructures patterned on a flat plasmonic metal have also been utilized to control the wavefronts of SPPs, yielding fascinating effects including SPP beam guiding [10,11], plasmonic Airy beams [12,13], near-field focusing [14–16] and holograms [17,18]. However, these devices were based on either transportation phase accumulations or Bragg scatterings of SPP waves, which inevitably suffer from the issues of their wavelength-scale size, low efficiencies, and/or limited functionalities.

Recently, gradient metasurfaces, consisting of planar microstructures (*i.e.*, meta-atoms) arranged in a specific order with tailored EM responses, have exhibited unprecedented capabilities to control EM waves [19]. Via structural adjustment, one can design metasurfaces exhibiting arbitrary phase retardations to reshape the wavefronts of impinging waves based on the Huygens' principle. Many wavefront reshaping effects, such as anomalous light bending [20–22], surface wave excitations [23–27], flat lensing [28–31], and meta-holograms [32–34], have been demonstrated based on metasurfaces. However, most works only focus on manipulating space waves. Very recently, we proposed using meta-walls, by analogy with

(a) These authors contributed equally to this work.
(b) E-mail: sls@fudan.edu.cn

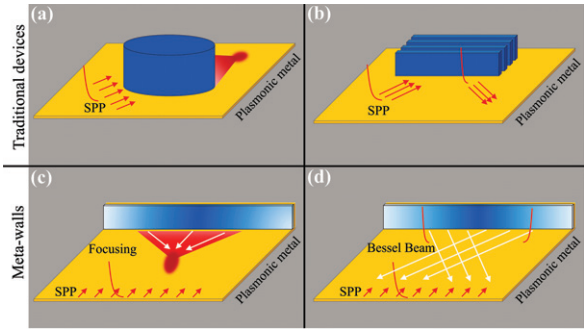

Fig. 1: (Colour online) Wavefront controls of SPPs with traditional optical elements and artificial meta-walls. (a) A cylindrical dielectric disk for SPP focusing. (b) A Bragg mirror for SPP reflection. (c), (d): the ultrathin meta-walls with specific reflection phase profiles for SPP focusing (c) and Bessel beam generation (d).

metasurfaces for space waves, to manipulate the wavefronts of SPPs [35]. Our primary experimental results on anomalous SPP reflections have demonstrated the validity of the proposed concept. However, SPP beams with complex wavefronts, which are particularly important for enhancing light-matter-interactions and nano-particle manipulations, have still not been achieved with the high efficiency and in a miniaturized scenario.

In this paper, we adopt the meta-wall strategy to achieve more sophisticated SPP manipulations, including SPP focusing and Bessel beams generations as shown in figs. 1(c), (d). We designed and fabricated two meta-walls exhibiting the desired reflection-phase distributions for spoof SPPs, and performed near-field measurements as well as finite-element-method (FEM) simulations to demonstrate the high efficiency and broadband functionalities of our devices. Compared with the conventional approaches for SPP controls, our meta-walls are ultrathin and flat, and exhibit higher efficiencies.

We first describe how to design the desired "meta-atoms" for constructing a meta-wall. In reflection geometry, the meta-atoms should reflect SPP waves with nearly 100% efficiency but with the reflection phases covering the whole 360° range dictated by their structures. Without loss of generality, we choose the microwave regime to verify our idea. Because natural SPPs do not exist in this regime, we designed an artificial plasmonic metal by covering a 2 mm thick dielectric slab ($\varepsilon = 2.65$) with a metallic mirror to support spoof SPPs (or guided surface waves) [23,36]. We then designed a series of homogeneous meta-walls, each consisting of a metal film covered by a 5 mm thick high-index ($\varepsilon = 16$) slab drilled with a periodic array (periodicity $P = 3$ mm) of subwavelength air holes (with varying diameters D)[1]. We finally placed such meta-walls vertically on the artificial plasmonic metal to study their reflection coefficients for the incident SPPs, as

[1]The height of the meta-wall is slightly larger than the decay length of the spoof SPPs to ensure a high reflection amplitude.

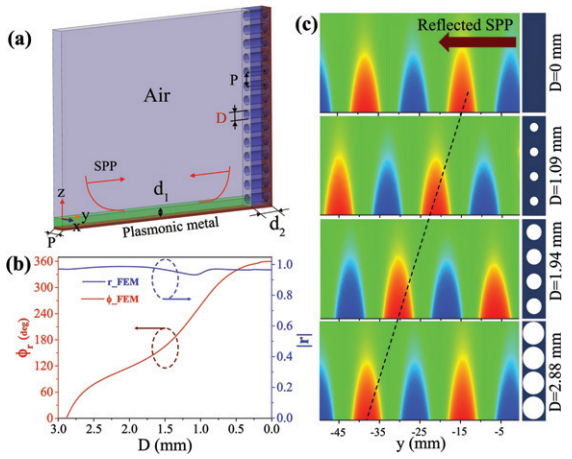

Fig. 2: (Colour online) Reflection phase modulation of spoof SPPs with a homogeneous meta-wall. (a) Simulation setup to obtain the SPP reflection coefficient of the uniform meta-wall, composed of a 5 mm thick high index slab ($\varepsilon = 16$) drilled with a subwavelength air hole array (periodicity $P = 3$ mm) and a PEC mirror. The spoof SPP is launched from the left boundary and propagate on the plasmonic metal, which is composed of a 2 mm thick dielectric spacer ($\varepsilon = 2.65$) capped on a PEC mirror. Periodic boundaries are set along the x-direction to describe an infinitely large system. (b) Simulated spoof SPP reflection amplitude and phase *vs.* diameter D. (c) Simulated reflected E_z field patterns from the meta-walls with a series of D values. Here, the frequency is fixed at 12 GHz.

shown in fig. 2(a). Figure 2(b) depicts the FEM-simulated SPP reflection coefficients, including both the amplitude and phase, for the designed meta-walls with different air-hole diameter D at 12 GHz. Simulations show that the eigen wave vector of the spoof SPP is $k_{\rm spp} = 1.055k_0$ with k_0 being the free-space wave vector. It is clear that, as D varies from 3 mm to 0 mm, the SPP reflection phase increases continuously covering the full 360° range, while the reflection amplitude is higher than 0.93. Figure 2(c) illustrates the simulated E_z field (real part) patterns (with incident SPP fields purposely subtracted) inside the systems with D set as 0 mm, 1.09 mm, 1.94 mm and 2.88 mm, respectively. As expected, the SPP waves reflected by the different systems do exhibit the desired phase retardations, suggesting that they are suitable meta-atoms to build inhomogeneous meta-walls for controlling the wavefront of SPPs. In particular, our simulations revealed that the scatterings of SPPs to space waves were negligible (fig. 2(c)), ensuring the high working efficiencies of the meta-devices that were built later. The working principle of these meta-atoms can be explained by the effective medium theory. Simply put, decreasing the D value can increase the effective index of the meta-wall, which, in turn, leads to an increased phase retardation for reflected SPPs [35]. To be noted, the height of the meta-wall does not need to be very large, as long as it is larger than the decay length of the SPPs. Beyond this value, the performance of the device is still quite good and robust, which is an obvious advantage in the practical applications.

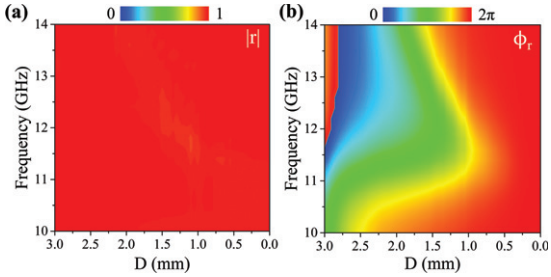

Fig. 3: (Colour online) Simulated SPP reflection amplitude (a) and phase (b) for the dielectric meta-wall *vs.* diameter D (x-axis) and frequency (y-axis). Here, the reflection phases at $D = 0$ are all shifted to 360° to facilitate the comparison between different frequencies.

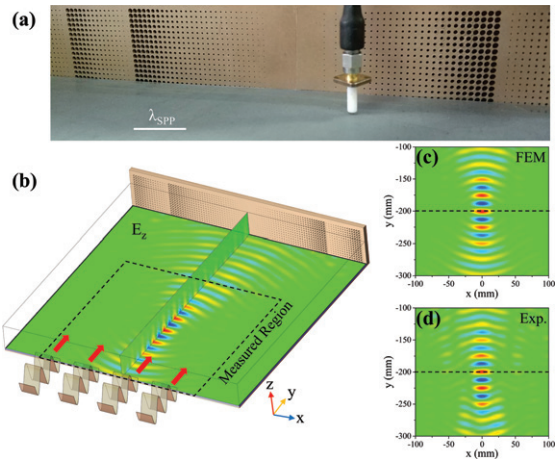

Fig. 4: (Colour online) Characterizations of the SPP meta-lens. (a) Image of part of the experimental setup, including the meta-wall, plasmonic metal, and a monopole antenna as near-field detector. (b) FEM-simulated reflected E_z field pattern above the plasmonic metal as the meta-wall is illuminated normally by a SPP wave. (c), (d): top view of the reflected E_z field above the plasmonic metal within the same measured region obtained by FEM simulations (c) and near-field measurements (d). Here, the frequency is 12 GHz.

Our designed meta-atoms can work efficiently within a broad frequency band. Figure 3 depicts the FEM-simulated amplitude and phase of the spoof SPP reflected by the meta-walls with varying air-hole diameter D (x-axis), at different frequencies (y-axis). It can be seen that the SPP reflection amplitude remains at high values within the whole frequency band (10–14 GHz), implying the robustness of the high-efficiency functionality of our devices. Moreover, the SPP reflection phase can always cover the full 360° range within the frequency range of (11.6–14 GHz). Because the effective permittivity of the capping layer are dispersionless [35], the SPP phase retardations accumulated inside the meta-wall must get smaller at lower frequencies, which explains why there exists a low-frequency limit for the system to yield a full 360° reflection phase coverage, as shown in fig. 3(b).

Knowing the properties of all meta-atoms as presented in fig. 3, we can use them to construct inhomogeneous meta-walls exhibiting appropriate phase profiles to reshape the wavefronts of SPPs efficiently. We first designed a SPP meta-lens exhibiting a parabolic reflection phase profile:

$$\phi\,(\mathrm{x}) = k_{\mathrm{spp}}\left(\sqrt{x^2 + F^2} - F^2\right), \qquad (1)$$

where $F = 200$ mm is the focal length at the central working frequency 12 GHz. According to eq. (1) and fig. 3, we can easily determine the geometrical parameters (D) of the required meta-atoms to construct our meta-lens. We first employ FEM simulations to demonstrate the SPP focusing effect as shown in fig. 4(b). In our simulations, we launched a Gaussian SPP beam on the plasmonic metal far away from the meta-lens, and studied how the SPP beam is reflected back by the meta-lens. The calculated reflection E_z field pattern on a plane 2 mm above the plamsonic metal clearly demonstrates the desired SPP focusing effect as shown in fig. 4(b). Here, the incident SPP field was also purposely subtracted from the total field, in order to prevent its interference with the reflected SPP beam. One can clearly identify a focal point at 200 mm, which agrees well with our theoretical predictions.

Encouraged by our simulation results, we then performed near-field scanning measurement to verify the performance of the meta-lens. Figure 4(a) depicts a part of the picture of our experimental setup, including the artificial plasmonic metal, the meta-lens, and the monopole antenna for near-field mapping. In our experiment, a SPP beam is excited on the plasmonic metal by a gradient meta-coupler [23], which then propagates on it and finally strikes the meta-wall. A monopole antenna is moved on a plane 2 mm above the plasmonic metal to measure the E_z field pattern. Figure 4(d) depicts the measured E_z field pattern corresponding only to the reflected SPP waves. Limited by our experimental setup, the measured area was only $200 \times 200\,\mathrm{mm}^2$. Comparisons between fig. 4(c) and (d) reveal the nice agreement between our measured and simulated results.

The proposed SPP meta-lens possesses a broad frequency band. Figure 5 compares the reflected SPP field patterns (including $|E_z|^2$ and E_z) above the plasmonic metal at five different frequencies, under exactly the same condition as those shown in fig. 4. A robust SPP focusing effect was obtained within the entire frequency band (12–14 GHz), although at frequencies away from the central working one (12 GHz) the focusing quality becomes deteriorated and the resulting focusing length was also different from the designed value (200 mm). To understand these effects, we show in figs. 5(a1)–(a5) the calculated reflection phase profiles of the meta-lens at five corresponding frequencies. While an ideal phase profile is obtained only at 12 GHz, the phase profiles at other frequencies still resemble a parabolic distribution, as expressed in eq. (1), but with a re-defined focal length that becomes shorter

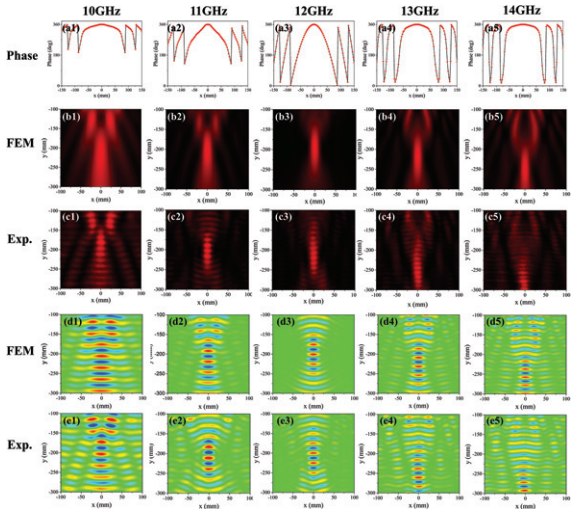

Fig. 5: (Colour online) Broadband performance of the SPP meta-lens. (a) SPP reflection phase profile for the meta-lens. (b)–(e) The reflected field pattern (including $|E_z|^2$ ((b), (c)) and E_z ((d), (e))) above the plasmonic metal, obtained via simulations ((b), (d)) and near-field measurements ((c), (e)). The five frequencies chosen here are 10–14 GHz.

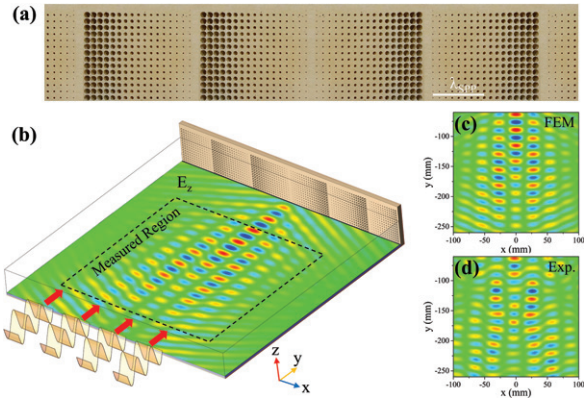

Fig. 6: (Colour online) Characterizations of the meta-wall for plasmonic Bessel beam generation. (a) Picture of a part of the fabricated SPP meta-lens. (b) FEM simulated reflected E_z field pattern when the meta-wall was illuminated normally by a SPP wave. (c), (d): top view of the reflected E_z field pattern above the plasmonic metal within the same measured region, obtained via simulations (c) and near-field experiments (d). Here, the frequency is 12 GHz.

at higher frequencies. However, at frequencies much lower than 12 GHz (*e.g.*, fig. 5(a1)), we note that $\phi(x)$ could not cover the full 360° range and deviates significantly from the ideal parabolic profile, which resulted in a deteriorated focusing effect.

The concept of meta-wall can be employed to generate SPP beams with arbitrarily complicated wavefronts. Here we show the generation of the SPP Bessel beam as an illustration. Because a three-dimensional Bessel beam is essentially a linear combination of all plane waves propagating at the same oblique angle (but with all possible azimuthal angles) with respect to a central axis, a SPP Bessel beam is a two-dimensional version containing two obliquely propagating SPP plane waves. Therefore, we need to design a meta-wall exhibiting the following reflection phase profile:

$$\phi\,(\mathrm{x}) = k_{\mathrm{spp}} \sin\theta\,|x|\,, \tag{2}$$

where θ denotes the defection angle of the two SPP plane waves. Knowing the desired phase distribution expressed in eq. (2), we can again determine the needed meta-atoms based on fig. 3 and then use them to construct a meta-wall for Bessel beam generations. Figure 6(a) shows the picture of the sample fabricated based on our design. The whole device contains 14 rows of air holes with their diameters varying from 0 mm to 2.83 mm, yielding a desired reflection phase profile expressed in eq. (2) with phase gradient $\xi = \pm 0.44 k_{\mathrm{spp}}$, at the working frequency 12 GHz. According to the generalized Snell's law for SPP [35], a normally incident SPP wave will be split into two SPP plane beams with opposite deflection angles $\theta \approx 26°$, and their interference forms the desired SPP Bessel beam.

We first employed FEM simulations to demonstrate the performance of our device. Figure 6(b) depicts the FEM-simulated E_z field pattern for the reflected SPP wave, as the meta-wall is illuminated by a normally incident SPP beam. It can be seen that the two non-specularly reflected SPP beams interfere with each other, forming a SPP Bessel beam. Due to the finite-size effect of the meta-wall, the two interfering SPP beams exhibit finite widths and, therefore, will separate eventually, leaving only a finite length exhibiting a non-diffraction characteristic.

Based on the same experimental setup as depicted in fig. 4, we measured the reflected E_z field pattern above the plasmonic metal, when the meta-wall was illuminated by an impinging SPP at 12 GHz. Our near-field scanning experimental results shown in fig. 6(d) are in reasonable agreement with our FEM simulations shown in fig. 6(c), undoubtedly illustrating the ability of our meta-wall to generate a SPP Bessel beam. The broadband functionality of the adopted meta-atoms ensure that the current Bessel beam generator also exhibits a broadband performance [35].

In summary, we extended the meta-wall concept to construct two high-efficiency meta-devices (*i.e.*, a SPP meta-lens and a Bessel beam generator) that can generate SPP beams exhibiting complex wavefronts. Both near-field measurements and full-wave simulations collectively demonstrated the good performances of our devices. Compared with the conventional approaches for manipulating SPPs, the proposed metal-walls can reshape the SPP's profile with higher frequency and more flexible functionalities in the subwavelength scale. This idea can stimulate research in numerous SPP-related fields at various frequency regimes, such as the enhanced nonlinear effect, bio- or chemical sensing, near-field imaging, nano-particle trapping, and so on.

* * *

This work was supported by the National Natural Science Foundation of China (Nos. 11404063, 11474057, 11734007, 11774064, 11674068), the National Key Research and Development of China (2017YFA0303500, 2017YFA0700200), and Shanghai Science and Technology Committee (Nos. 18ZR1403400, 16ZR1445200, 16JC1403100).

REFERENCES

[1] Fang N., Lee H., Sun C. and Zhang X., *Science*, **308** (2005) 534.
[2] Kim S., Jin J., Kim Y.-J., Park I.-Y., Kim Y. and Kim S.-W., *Nature*, **453** (2008) 757.
[3] Kauranen M. and Zayats A. V., *Nat. Photon.*, **6** (2012) 737.
[4] Oulton R.-F., Sorger V. J., Zentgraf T., Ma R.-M., Gladden C., Dai L., Bartal G. and Zhang X., *Nature*, **461** (2009) 629.
[5] Zia R., Schuller J.-A., Chandran A. and Brongersma M.-L., *Mater. Today*, **9** (2006) 20.
[6] Hohenau A., Krenn J. R., Stepanov A.-L., Drezet A., Ditlbacher H., Steinberger B., Leitner A. and Aussenegg F.-R., *Opt. Lett.*, **30** (2005) 893.
[7] Devaux E., Laluet J.-Y., Stein B., Genet C., Ebbesen T., Weeber J.-C. and Dereux A., *Opt. Express*, **18** (2010) 20610.
[8] Feng L., Lu M.-H., Lomakin V. and Fainman Y., *Appl. Phys. Lett.*, **93** (2008) 4.
[9] Randhawa S., González M. U., Renger J., Enoch S. and Quidant R., *Opt. Express*, **18** (2010) 14496.
[10] Radko P., Evlyukhin A. B., Boltasseva A. and Bozhevolnyi S. I., *Opt. Express*, **16** (2008) 3924.
[11] Ditlbacher H., Krenn J. R., Schider G., Leitner A. and Aussenegg F.-R., *Appl. Phys. Lett.*, **81** (2002) 1762.
[12] Minovich A., Klein A.-E., Janunts N., Pertsch T., Neshev D.-N. and Kivshar Y.-S., *Phys. Rev. Lett.*, **107** (2011) 116802.
[13] Li L., Li T., Wang S. M., Zhang C. and Zhu S.-N., *Phys. Rev. Lett.*, **107** (2011) 126804.
[14] Drezet A., Stepanov A. L., Ditlbacher H., Hohenau A., Steinberger B., Aussenegg F.-R., Leitner A. and Krenn J.-R., *Appl. Phys. Lett.*, **86** (2005) 74104.
[15] Yin L., Vlasko-Vlasov V.-K., Pearson J., Hiller J. M., Hua J., Welp U., Brown D.-E. and Kimball C.-W., *Nano Lett.*, **5** (2005) 1399.
[16] Li L., Li T., Wang S., Zhu S. and Zhang X., *Nano Lett.*, **11** (2011) 4357.
[17] Ozaki M., Kato J. and Kawata S., *Science*, **332** (2011) 218.
[18] Chen Y.-G., Chen Y.-H. and Li Z.-Y., *Opt. Lett.*, **39** (2014) 339.
[19] Yu N. and Capasso F., *Nat. Mater.*, **13** (2014) 139.
[20] Yu N., Genevet P., Kats M.-A., Aieta F., Tetienne J.-P., Capasso F. and Gaburro Z., *Science*, **334** (2011) 333.
[21] Ni X., Emani N.-K., Kildishev A.-V., Boltasseva A. and Shalaev V.-M., *Science*, **335** (2012) 427.
[22] Sun S., Yang K.-Y., Wang C.-M., Juan T.-K., Chen W.-T., Liao C.-Y., He Q., Xiao S., Kung W.-T., Guo G.-Y., Zhou L. and Tsai D.-P., *Nano Lett.*, **12** (2012) 6223.
[23] Sun S., He Q., Xiao S., Xu Q., Li X. and Zhou L., *Nat. Mater.*, **11** (2012) 426.
[24] Lin J., Mueller J.-P. B., Wang Q., Yuan G., Antoniou N., Yuan X.-C. and Capasso F., *Science*, **340** (2013) 331.
[25] Pors A., Nielsen M.-G., Bernardin T., Weeber J.-C. and Bozhevolnyi S.-I., *Light: Sci. Appl.*, **3** (2014) e197.
[26] Sun W., He Q., Sun S. and Zhou L., *Light: Sci. Appl.*, **5** (2016) e16003.
[27] Duan J., Guo H., Dong S., Cai T., Luo W., Liang Z., He Q., Zhou L. and Sun S., *Sci. Rep.*, **7** (2017) 1354.
[28] Li X., Xiao S., Cai B., He Q., Cui T.-J. and Zhou L., *Opt. Lett.*, **37** (2012) 4940.
[29] Chen X., Huang L., Muhlenbernd H., Li G., Bai B., Tan Q., Jin G., Qiu C.-W., Zentgraf T. and Zhang S., *Adv. Opt. Mater.*, **1** (2013) 517.
[30] Khorasaninejad M., Chen W.-T., Devlin R.-C., Oh J., Zhu A.-Y. and Capasso F., *Science*, **352** (2016) 1190.
[31] Wang S., Wu P. C., Su V.-C., Lai Y.-C., Chu C.-H., Chen J.-W., Lu S.-H., Chen J., Xu B., Kuan C.-H., Li T., Zhu S. and Tsai D.-P., *Nat. Commun.*, **8** (2017) 187.
[32] Chen W.-T., Yang K., Wang C., Huang Y., Sun G., Liao C.Y., Hsu W., Lin H.-T., Sun S., Zhou L., Liu A. Q. and Tsai D.-P., *Nano Lett.*, **14** (2014) 225.
[33] Zheng G., Mühlenbernd H., Kenney M., Li G., Zentgraf T. and Zhang S., *Nat. Nanotechnol.*, **10** (2015) 308.
[34] Ni X., Kildishev A.-V. and Shalaev V.-M., *Nat. Commun.*, **4** (2013) 2807.
[35] Dong S., Zhang Y., Guo H., Duan J., Guan F., He Q., Zhao H., Zhou L. and Sun S., *Phys. Rev. Appl.*, **9** (2018) 14032.
[36] Lockyear M., Hibbins A. and Sambles J., *Phys. Rev. Lett.*, **102** (2009) 73901.